Title: Increased rates of hybridization in swordtail fish are associated with water pollution

Authors:

Benjamin M Moran[1,2,3†], Wilson F Ramírez-Duarte[2,4,5], Daniel L Powell[1,2,6], Terrance TL Yang[1], Theresa R Gunn[1,2], Gaston I Jofre-Rodríguez[2,7], Cheyenne Y Payne[8,9], Erik NK Iverson[10], Gabriel A Preising[1,2], Shreya M Banerjee[3], Alexandra E Donny[1,11], Rhea Sood[1], John J Baczenas[1], Gabriela María Vázquez Adame[2], Carla Gutiérrez-Rodríguez[12], Chelsea M Rochman[4], Molly Schumer[1,2,13*†], Gil G Rosenthal[2,14*]

Affiliations:

[1] Department of Biology, Stanford University

[2] Centro de Investigaciones Científicas de las Huastecas "Aguazarca", A.C.

[3] Present Address: Department of Evolution and Ecology, University of California at Davis

[4] Department of Ecology & Evolutionary Biology, University of Toronto

[5] Present Address: Department of Environmental & Physical Sciences, Concordia University of Edmonton

[6] Department of Biological Sciences, Louisiana State University

[7] Department of Biology, Virginia Commonwealth University

[8] Department of Ecology and Evolutionary Biology, University of California, Santa Cruz

[9] Southwest Fisheries Science Center, National Marine Fisheries Service, National Oceanic and Atmospheric Administration

[10] Department of Integrative Biology, University of Texas at Austin

[11] Department of Genome Sciences, University of Washington

[12] Red de Biología Evolutiva, Instituto de Ecología A.C

[13] Freeman Hrabowski Fellow, Howard Hughes Medical Institute

[14] Dipartimento di Biologia, Università di Padova

* co-supervised this work

[†] Correspondence: bmmoran@ucdavis.edu, schumer@stanford.edu

Running Head: Anthropogenic hybridization in swordtails

Keywords: hybridization, hybrid populations, anthropogenic change, water quality, mate choice, freshwater fish, swordtail fish, land use

Abstract

The nature of reproductive barriers which separate species is a fundamental question of evolutionary biology. Such barriers may be sensitive to environmental conditions, and recent research has documented an increasing number of cases where anthropogenic environmental disturbance is associated with new hybrid populations. However, few studies have been able to quantitatively compare potential environmental drivers and test possible mechanisms connecting interspecific hybridization to anthropogenic disturbance. Here, we combine genomic and chemical surveys to explore the loss of reproductive isolation between the sister species *Xiphophorus malinche* and *X. birchmanni*, fishes whose riverine habitat in the Sierra Madre Oriental of Mexico is increasingly impacted by human-mediated disturbance. By sequencing whole genomes of thousands of fish, we characterize the landscape of hybridization between these species in four distinct streams. Ancestry structure varied dramatically across streams, ranging from stable coexistence to clinal hybrid zones, hinting that dynamics of hybridization in this system may be environmentally dependent. In one stream, a sudden shift in patterns of hybridization coincides with the stream's passage through an urbanized area, with upstream sites showing distinct ancestry clusters and downstream sites showing a swarm of hybrids with variable ancestry. Water chemistry measurements show that water quality changes significantly over this area, including in parameters known to disrupt fish olfaction and mating. We hypothesize that the hybrid swarm downstream of the town is driven by disruption of olfaction that impacts mating preferences. By sequencing mothers and embryos, we show that there is reduced assortative mating at sites downstream of the urbanized area compared to strong assortative mating at upstream sites. We identify alterations of the olfactory epithelium at the

same downstream site which are consistent with chemical irritation from polluted waters. Taken together, our work illuminates the mechanisms linking anthropogenic disturbance to the breakdown of reproductive isolation in these hybridizing species.

Introduction

To understand speciation, evolutionary biologists have long studied cases in which barriers to reproduction between species are incomplete and hybridization can occur (1, 2). Such studies have sometimes found evidence that hybridization occurs in areas of environmental disturbance. Disturbance can bring together species which do not otherwise coexist, create novel environments where hybrids thrive, or alter the interactions between species that previously coexisted without interbreeding (3–5). Empirical work has shown that premating barriers, such as a behavioral preference for mating with conspecifics (i.e. assortative mating) are highly context-dependent (6–10) and sensitive to environmental conditions (11, 12). These barriers may therefore disappear in the face of disturbances that impact mechanisms of mate discrimination (13–15). Such "premating" barriers often arise early in the divergence of two lineages (16, 17) and thus may be especially important in the origin and preservation of biodiversity (18–20).

While natural changes to the environment may have been the major source of disturbance historically, human impacts (e.g. changes in land use, chemical pollution, resource extraction) have likely played an analogous role in recent decades (14, 21–23). Human modification of the environment can interfere with mechanisms used by conspecifics to identify each other, either by directly affecting signal production or transmission or by abolishing conspecific preferences (14, 24, 25). In aquatic species, in particular, a variety of chemical pollutants have been shown to weaken or ablate conspecific mate preferences (14, 24–28). As human impacts on the environment become ubiquitous (29), the reported rate of hybridization appears to be increasing across a range of taxa (5).

If assortative mating is a major reproductive barrier between species, weakening this barrier can lead to a sudden collapse of population structure and phenotypic divergence (30–34), often referred to as a “hybrid swarm”. Since mate discrimination is typically weaker in hybrids than in parental species (13), this can lead to irreversible phenotypic and genetic homogenization through hybridization (i.e. “speciation reversal” or “genetic swamping”). Although hybridization may sometimes lead to the formation of new species (35), hybrid speciation without a change in chromosome number appears to be relatively rare (36), and the immediate consequence of the formation of hybrid swarms is more often the loss of genetic differentiation and functional biodiversity (1, 23). Moreover, early-generation hybrids often experience reduced fitness due to intrinsic hybrid incompatibilities (37, 38) between the parental genomes (although we note that hybridization can also facilitate adaptation; (39, 40)). Thus, in addition to its direct effects of homogenizing divergent species, hybridization may also decrease overall population size and fecundity.

Swordtails (Teleostei: genus *Xiphophorus*) provide a compelling system in which to study the barriers to gene flow in natural populations and their breakdown following anthropogenic disturbance. As model systems for hybridization and mate choice, these stream fishes are the subject of numerous studies showing that mating preferences can be altered by environmental and social context (7, 8, 13, 24). Swordtails are found in the eastern slopes of the Sierra Madre Oriental and Gulf coastal plain of Mexico, a region experiencing growing human population density and agricultural land conversion since the 20th century (41, 42). This change in land use has impacted water quality in the region, while also threatening the area’s exceptional biodiversity (43, 44). In particular, the sister species *X. malinche* and *X. birchmanni* overlap in the montane streams of northern Hidalgo state, Mexico, where steep slopes create frequent

111 barriers to migration (waterfalls, cascades, and subterranean stream reaches) and coincide with
112 dramatic ecological variation over short geographic distances. *X. malinche* occupy cool
113 headwater streams while *X. birchmanni* are found in warmer lower-elevation streams, creating
114 the potential for ecological selection against hybrids (45, 46). In addition, early-generation
115 hybrids between these species suffer from severe genetic incompatibilities (47–49). However,
116 some hybrids are viable and fertile, and natural hybrid zones can be found in multiple
117 independent stream reaches (50, 51). Researchers first reported hybridization between *X.*
118 *malinche* and *X. birchmanni* in 1997, whereas hybrids were not detected when sampling the
119 same stream reaches a decade earlier (52, 53). Meanwhile, the period of 1980–1995 saw a 37%
120 increase in human population in the state of Hidalgo (54). Independent genetic approaches have
121 estimated that these hybrid zones are on the order of ~100 generations old (55), consistent with
122 hybridization beginning in the late 1900s. This recent onset of hybridization begs the question of
123 what triggered it, and whether it was tied to the concurrent socio-ecological transformation of the
124 region.

125 Though we lack ecological data from these streams prior to the start of hybridization,
126 spatial patterns in present day populations may provide insights into the drivers of hybridization.
127 The genetic structure in most hybrid populations between *X. malinche* and *X. birchmanni* is best
128 described as a hybrid swarm lacking population structure (50). One exception to this pattern
129 among described populations is a stream reach just upstream of the town of Calnali, Hidalgo.
130 There, genetic studies have described two subpopulations of *malinche*-like and *birchmanni*-like
131 admixed fish that exist in sympatry (Fig. 1; (56). Sequencing over multiple years showed that
132 this bimodal population structure has been stable over time, and is driven by strong assortative
133 mating between individuals of the same ancestry group (56). However, recent sampling showed

that population structure disappears just downstream of the town of Calnali (47), raising the possibility that assortative mating breaks down after exposure to a point pollution source.

Here, we use whole-genome sequencing of 2620 fish and comprehensive surveys of water chemistry to study the relationship between environmental conditions and patterns of hybridization across multiple *X. malinche* × *X. birchmanni* hybrid zones in Hidalgo, Mexico. We survey hybrid ancestry in four streams and compare hybrid population structure across demographically independent hybrid zones. We find that assortative mating between ancestry clusters in the Río Calnali breaks down at the precise point where anthropogenic inputs drastically change water chemistry, leading to a sudden change in population structure. Based on comprehensive water chemistry measurements, we identify multiple pollutants which spike at the point of population structure collapse. This pattern of population structure collapse is unique to the Rio Calnali; other stream systems show little change in population structure over broad geographic distances. Using land use classification of satellite imagery, we confirm that these changes in water chemistry downstream on the Río Calnali are coupled with a uniquely high density of built infrastructure in close proximity to the stream. Given the known importance of olfactory communication in swordtail mate choice, we test for evidence of damage to olfactory rosettes as a result of exposure to pollutants. We find evidence of greater histological damage in samples from polluted sites compared to less disturbed sites. This work thus establishes a quantitative link between environment, phenotype, and genomics in an anthropogenic hybrid zone, deepening our understanding of human impacts on biodiversity.

Materials and Methods

Study area and sample collection

We collected fin clips from 44 sites across four stream basins which together compose the Río Atlapexco drainage of Hidalgo, Mexico (see Table S1 for full list with GPS coordinates) for low-coverage whole genome sequencing. Fish were collected using baited minnow traps and anesthetized in a buffered solution of 100 mg/mL MS-222 dissolved in stream water (Stanford APLAC protocol #33071). Fish were allowed to recover after fin clips were collected, then were returned to the pool from which they had been sampled. Tissue was stored in 95% ethanol for DNA extraction. A subset of female fish from the Calnali Mid (n = 22) and Calnali Low (n = 74) populations (Fig. 1) were euthanized and stored with their embryos in 95% ethanol for analysis of assortative mating (see below). In addition, 30 fish each from the Aguazarca and Calnali Low populations were decapitated following euthanasia, with whole heads preserved in 10% neutral buffered formalin for olfactory histology (see below).

DNA extraction and coverage whole-genome sequencing

DNA was extracted from preserved fin clips using the Agilent DNAdvance extraction kit (Beckman Coulter, Brea, California). The protocol followed the manufacturer's instructions for tissue extraction except that we used half-reactions. Extracted DNA was quantified on a BioTek Cytation5 (Agilent, Santa Clara, CA) microplate reader and diluted to 10 ng/µl for library preparation. We used a previously described tagmentation-based protocol to prepare DNA for

177 sequencing (45). Libraries were dual-indexed via amplification (12 PCR cycles) and purified
178 using 18% SPRI beads. Libraries were quantified on a Qubit fluorometer (Thermo Scientific,
179 Wilmington, DE) and library size distribution was visualized on an Agilent 4200 Tapestation
180 (Agilent, Santa Clara, CA). Libraries were sequenced at Weill Cornell Medical College, Harvard
181 Bauer Core, and Admera Health Services (South Plainfield, NJ).
182
183 *Local ancestry inference*
184
185 Hybrids between *X. birchmanni* and *X. malinche* harbor ancestry from both species that
186 varies locally along the genome and globally between individuals and populations. We used an
187 approach developed by our group for accurate local ancestry inference in *X. malinche* × *X.*
188 *birchmanni* hybrids that relies on a hidden Markov model and known ancestry informative sites
189 that distinguish *X. birchmanni* and *X. malinche* to infer local ancestry (*ancestryinfer*; (57)). Both
190 simulation studies (57) and analyses of populations of known ancestry have indicated that this
191 approach has a low error rate (~0.1% per ancestry informative site (48, 58)). Likewise, inference
192 of local ancestry is robust to a number of technical challenges including parameter
193 misspecification (57).
194 We inferred local ancestry using *ancestryinfer* from whole genome sequence data for all
195 individuals for which we collected more than 300,000 reads from the sequencing approach
196 described above. This coverage cutoff is based on previous simulation studies (57) and resulted
197 in 12 to 702 individuals per site post-filtering (median 32; Table S1). *Ancestryinfer* outputs
198 posterior probabilities of ancestry for all informative sites along the genome. In the case of *X.*
199 *malinche* × *X. birchmanni* hybrids, this results in estimates of ancestry at 729,167 ancestry

200 informative sites across 24 chromosomes. Since we were primarily interested in accurately
201 estimating global admixture proportion for individuals along a spatial cline, we converted
202 posterior probabilities to 'hard calls' using a threshold of 0.9. For example, if an individual had a
203 posterior probability greater than or equal to 0.9 for *X. malinche* ancestry at a given marker, we
204 converted that marker to the *X. malinche* state. If a site did not have a posterior probability ≥0.9
205 for any ancestry state, we converted the site to missing data.

206 We used these hard calls to estimate the proportion of the genome derived from each
207 parental species. We estimated this proportion using two approaches. First, we calculated the
208 ratio of the number of alleles called for the *X. malinche* state out of the total number of alleles
209 called (treating heterozygous sites as 1 allele for each parental species). We also used a spatially
210 aware approach, given that there is variation in the distance between ancestry informative sites.
211 To do so, we calculated the proportion of the genome covered by high-confidence *X. malinche* or
212 *X. birchmanni* ancestry tracts, excluding regions that were not confidently called from the
213 denominator. In practice, this approach generated nearly identical results (Supp. Info. 1; Fig. S1).

214 With these results in hand, we visualized the distribution of admixture proportion in
215 populations along the Río Calnali, Río Pochula, Río Huazalingo, and Río Conzintla (Fig. 2). As
216 previous results had indicated the presence of bimodal ancestry structure in upstream populations
217 of the Río Calnali, we also calculated Hartigan's dip statistic (59), which quantifies departures
218 from a unimodal distribution, on samples from each collection site. Since we used this test across
219 many sites, we applied a Bonferroni correction for the number of tests. Samples were collected
220 between 2006 and 2024, with the highest sampling density between 2014 and 2022 (Table S2).
221 Given the broad time period over which samples were collected, we also evaluated whether
222 ancestry structure was stable at a given site across the study period (Supp. Info. 2; Fig. S2; (56).

Water chemistry surveys

We chose to focus water quality sampling on a subset of 32 sampling sites that captured the full range of variation in ancestry structure present in each stream and collected multimodal measurements from these sites between February 2022 and September 2024 (Fig. 1). Due to changes in equipment availability over time, sample sizes for individual water quality measurements varied between 0 and 13 per location and measure; for details on all measures collected and sample sizes per location, see Table S3. We measured temperature, conductivity, dissolved oxygen, and fluorescent dissolved organic matter (fDOM) using YSI EXO 2 and EXO 1s multiparameter sondes (Xylem Inc.). Turbidity was measured in nephelometric turbidity units (NTUs) with an Orion AQ4500 Turbidity Meter (Thermo Fisher). Using a YSI 9500 photometer, we applied colorimetric assays to measure pH, total alkalinity, total hardness, calcium hardness, and concentrations of sulfate, sulfite, sulfide, phosphate, ammonia, nitrite, and nitrate. Sonde measurements, turbidity measurement, and colorimetry tests were performed at the site of sampling to ensure the accurate measurement of unstable chemicals, while further measurements were performed on collected water samples. For measurements of dissolved organic carbon (DOC) and total nitrogen, we stored samples in glass vials capped with PTFE/silicone septa, which were combusted at 500 °C for 1 hour and rinsed ten times with ultrapure water (Milli-Q® Merck) prior to sample collection. Water samples were processed on-site by syringe-filtering through a 0.45 μm polyethersulfone (PES) membrane, acidifying to pH 2–3 using concentrated hydrochloric acid, and capping with no air bubbles remaining in the vial. DOC and N measurements were carried out on a Shimadzu TOC-L analyzer using the TC/IC and TN protocols, respectively, at the Environmental Engineering Laboratory of the National

Autonomous University of Mexico (UNAM) and the Environmental Measurements Facility at Stanford University. Total and dissolved metals were measured from samples collected in 50 mL Falcon tubes triple-rinsed with sample water, with samples for dissolved metals filtered through 0.45 μm PES and all samples acidified to a pH of ~2 using trace metal grade nitric acid. Inductively coupled plasma mass spectrometry (ICP-MS) detection of 39 ions was carried out following a modified version of the APHA3030B/6020A methods by ALS Environmental (Waterloo, ON; see Table S4 for full list of ions and QA/QC). Given that many metals in the filtered samples were below the lower detection limits of ICP-MS, we used ICP-MS measurements of total concentration from unfiltered samples in all downstream statistical analyses.

Geospatial Analyses

To complement our measurements of water chemistry, we measured land use in each stream catchment as a proxy for anthropogenic disturbance. Briefly, we used Google Earth Engine to access Sentinel-2 multispectral imagery from the month of May in the years 2020–2023 (60), removed images with > 20% cloud cover, masked pixels flagged as clouds, then took the median intensity for each band and pixel to construct a composite image with bands 11 (1610 nm, short-wave infrared, 20 m^2 resolution), 8 (842 nm, near-infrared, 10 m^2), and 2 (490 nm, blue, 10 m^2). This spectral combination provides better contrast between built infrastructure, herbaceous, and woody vegetation than the visible spectrum (61). All further analyses were performed in ArcGIS Pro (version 3.3.1) with the Spatial Analyst and Image Analyst extensions. We segmented the three-band raster file using the Segmentation tool, with a spectral detail of 18,

a spatial detail of 19, and a minimum size per object of 20 pixels. Next, we selected four land use types for classification: water, forest (continuous tree cover, excluding plantation-style agriculture), non-forest vegetation (grassland, pasture, or cultivated crops, including plantation-style orchard), and developed land (buildings, mines, and roads). We included water surfaces (primarily to prevent their misclassification as other land use types), forest as the primary undisturbed land cover in the area, and non-forest vegetation as an additional form of human disturbance beyond hardened infrastructure. Using 3 m^2-resolution imagery of the study area in March 2022 downloaded from Planet Labs (62), we identified 60 polygons of each land class to serve as training samples. Given the short time frame between the capture of our Sentinel and Planet Labs image sets, we assumed that there would be negligible change in the proportion of land classes. We then used the Classification tool to perform object-based land use classification using a support vector machine algorithm with maximum 500 samples per class. We visually inspected the resulting classification for pixels misclassified as developed land, and removed these pixels from the dataset prior to further analyses (0.8% of all pixels).

To delineate catchments for each sampling site, we downloaded a digital elevation model (DEM) of the state of Hidalgo with 15 m^2 resolution from the Mexican National Institute for Statistics and Geography (63). Starting with this DEM, we calculated flow direction and flow accumulation, snapped each site to the nearest pour point pixel, and calculated the land area which drained into the stream upstream of a given site (Fig. S3), using the Flow Direction, Flow Accumulation, Snap Pour Points, and Watershed tools, respectively. To identify the land area with greatest potential for runoff into waterways (i.e. greatest influence on water chemistry), we used the Raster Calculator tool. We converted all cells which received flow from at least 3000 uphill cells into a polyline object representing the relevant waterways in our study area (Fig. S3).

We then used the Buffer tool to identify the land area within 500 m, 100 m, and 50 m of these waterways, and used the Clip Raster tool to identify the subset of classified land use pixels within each of these buffers. Using the Zonal Histogram tool, we summed the pixel counts of each land use category in each site's subcatchment, then calculated the proportion of the total pixels per subcatchment composed of each land use type. Finally, we calculated cumulative land use within a site's watershed by summing the land use categories within its own site-specific subcatchment and within the subcatchments of all upstream sites.

Statistical analysis of environmental data

We explored overall differences in water chemistry between sites and drainages using Principal Component Analysis (PCA). Given differing sample sizes of ICP-MS measurement relative to other measures, we conducted two separate PCAs, one for ICP-MS metals measurement (n = 66 measurements) and one for all other data (n = 58). For water chemistry parameters other than metals, we included only measurements which were consistently collected throughout the length of the field study, including dissolved oxygen (mg/L), fDOM (quinine sulfate units), conductivity (μS/cm), total hardness (mg/L $CaCO_3$ equivalent), total alkalinity (mg/L $CaCO_3$ equivalent), pH, nitrite (mg/L N), ammonia (mg/L N), phosphate (mg/L PO_4), sulfate (mg/L SO_4), and turbidity (NTU). Of the 39 ions measured in the metals measurements, we retained 30 which had more than one measurement above the lower detection limits of ICP-MS. For the purposes of this analysis, metals measurements below the detection limit were set to halfway between zero and the lower detection limit. For example, for cadmium, the detection limit was 5 ng/L and we set values below the detection limit to 2.5 ng/L. While this approach has

some limitations (64, 65) compared to alternative approaches using imputation (66), we could not apply imputation approaches to our data given the possibility of systematic differences in concentrations of many of the metals between streams. However, we explored the potential impacts of this analysis choice on our conclusions by repeating PCAs with the measurements below the detection limit set to the detection limit or zero, and found our results were qualitatively unchanged (Fig. S4).

We also used the PCA analysis to qualitatively compare patterns within and across streams and identify chemicals of interest for further statistical analysis. Specifically, we chose chemicals which had negative loadings on both PC1 and PC2 in either the non-metal or metal PCA because we found that this approach clearly separated sites downstream on the Río Calnali from the others (Fig. 4). From this set of parameters, we next investigated which had evidence for affecting fish neurobiology, olfaction, or mate choice in the literature. These parameters included DOM (24), turbidity (67), nitrite (68), ammonia (69, 70), copper (71, 72), lead (73), cadmium (74, 75), zinc (76), and aluminum (77). In the analysis of ICP-MS metals data, where the effects of samples below the detection limit prevented the use of parametric tests, we used Kruskal-Wallis tests to identify differences in concentration within and between drainages. For all other variables, we used ANOVA and Tukey's HSD tests to confirm differences between the downstream Calnali sites and the other groups, testing for differences in the log-transformed response variables as a function of drainage, sampling month, and their interaction. We also used the same approach to explore differences in water chemistry between watersheds (Supp. Info. 3; Fig. S5–6) and over different years across the sampling period (Supp. Info. 4; Fig. S7–9).

Finally, we tested whether broad-scale variation in water chemistry was associated with variation in land use along the streams. We created a combined dataset of all parameters

338 described above, calculated the site-wise average of each water quality parameter across all
339 measurements, and then constructed a PCA (n = 30 sites). We found that the variation in the PCA
340 largely mirrored our prior analyses on subsets of the data discussed above (Fig. S10). We then
341 conducted two separate linear regressions with the top two principal components of water
342 chemistry variation as response variables, each as a function of five explanatory variables: the
343 site-specific and cumulative proportion of developed land upstream of the site, the site-specific
344 and cumulative proportion of non-forest vegetation upstream of the site, and the total watershed
345 area. We repeated our analyses considering only land use within 50 m of the closest point of the
346 stream, and also evaluated the effects of using different approaches to account for detection
347 limits in the ICP-MS measurements (setting measurements to the detection limit, zero, or a
348 random uniform variable drawn between zero and the detection limit; Table S10–12).
349
350 *Analysis of ancestry assortative mating in Calnali Low*
351
352 Previous work has shown that the vast majority of individuals above the town of Calnali
353 on the Río Calnali fall into one of two ancestry clusters: a *X. birchmanni* biased cluster that
354 derived ~75% of its genome from *X. birchmanni* and a *X. malinche* biased cluster that derives
355 >90% of its genome from *X. malinche*. These distinct ancestry clusters are maintained by strong
356 ancestry-assortative mating (56); note that in this prior work, samples from the nearby sites
357 Aguazarca and Calnali Mid were pooled for analysis, but we analyze them separately here (Fig.
358 1B). In the current study, we identify the Calnali Low population as one of the first sampling
359 sites where this genetic structure breaks down along the Río Calnali. As a result, we were

interested in evaluating the strength of ancestry assortative mating in this population and making comparisons to upstream populations.

To do so, we analyzed mother-embryo samples from the Calnali Low population, including previously published samples collected in 2020 (48), as well as newly sequenced samples from a 2017 collection, and compared them to mother-embryo pairs collected from populations upstream of the town of Calnali between 2008 and 2018. Because swordtails are livebearing fish which exhibit multiple paternity, when we collect pregnant *X. malinche* × *X. birchmanni* females we also collect ~10 offspring from 2-3 fathers (78). Although we cannot directly assay the paternal genotypes, we can use the ancestry of the offspring to infer the ancestry of the male that sired each embryo, since offspring will inherit approximately 50% of their genome from each parent. Thus, the difference between the mother's genome-wide ancestry and the genome-wide ancestry of her offspring is a useful proxy for paternal ancestry.

We have previously used this approach to quantify ancestry-assortative mating in upstream populations on the Río Calnali (56), and repeat this approach here. Specifically, we ask about the observed difference between maternal and offspring ancestry genome-wide in each population, compared to expectations under a scenario where females mate at random with respect to male ancestry. To generate a distribution of offspring ancestry expected under no assortative mating, we performed simulations. For each focal female in our dataset (n = 74 for Calnali Low, n = 22 for Calnali Mid), we randomly sampled a mate from our full dataset of adults from that population (n = 702 for Calnali Low, n = 79 for Calnali Mid). Next, we calculated the mean of the maternal and simulated paternal ancestry. We added noise to this average ancestry by sampling from a random normal distribution with the mean set to the variance in admixture proportion among full siblings observed in our data (Supp. Info. 6). We

383 repeated this procedure until we had simulated offspring for all of the focal females. We
384 generated 1,000 replicate simulations and compared the observed and simulated differences in
385 mother-offspring admixture proportions in each population. Finally, we compared the mean of
386 the difference in mother-offspring admixture proportions between the two populations using a
387 two-sample *t*-test.
388
389 *Inferring the strength of assortative mating from observed maternal-offspring ancestry*
390 *distributions*
391
392 We found evidence that the observed mother-offspring ancestry patterns in the Calnali
393 Low population differed subtly from patterns expected if mating were truly random with respect
394 to ancestry (Fig. 5A). However, this difference from random mating was much weaker than that
395 inferred in the population upstream of the town of Calnali (Fig. 5A). To quantitatively compare
396 the strength of ancestry-assortative mating consistent with the observed data, we used the same
397 approach previously used to quantify the strength of ancestry assortative mating at upstream sites
398 (56).
399 Briefly, we used an approximate Bayesian computation approach to evaluate what levels
400 of ancestry-assortative mating were consistent with our observed data. We drew a probability that
401 a female would accept a mate with an ancestry proportion that differed from hers by more than
402 5% (see Supp. Info. 6 for simulations using different thresholds) from a random uniform
403 distribution ranging from 0 (perfect assortative mating) to 1 (random mating). We refer to this
404 value as the strength of assortative mating. For each female we then randomly drew a mate from
405 the population ancestry distribution. If the mate fell within the ancestry threshold, the mate was

accepted. If it did not, we used a random binomial weighted by the strength of assortative mating to determine if the mate was accepted. If the mate was rejected, we continued this procedure until the female was matched with a mate, then simulated offspring as described above. This was repeated until all females were matched with a mate. We repeated this simulation procedure for a total of 3,000,000 simulations.

We used a simple rejection sampling approach to select simulations that closely matched the empirical data. For each simulation, we calculated the mean and variance of the difference in ancestry between mothers and their offspring. If both summary statistics fell within 5% of the observed value for the population (Calnali Low mean 6.6%, variance 0.46%; Calnali Mid mean 2.5%, variance 0.26%), we accepted the simulation. This allows us to estimate the range of values of assortative mating consistent with our data. We plotted the posterior distribution of accepted assortative mating strengths and identified the maximum a posteriori (MAP) estimate. We repeated this procedure with other thresholds of ancestry proportion differences (see Supp. Info. 6; Fig. S11). To evaluate whether results were affected by our approach in modeling assortative mating, we also explored an alternative approach modelling assortative mating as a continuous beta function (Supp. Info. 7; Fig S12). To test for a difference in the strength of assortative mating between populations, we first evaluated whether the inferred strength of assortative mating in one population fell within the 95% credible interval of the other population, and vice versa. To investigate whether the distributions were significantly different, we randomly matched each of the 1073 accepted simulations from Calnali Mid with one of the 5720 accepted simulations from Calnali Low, sampled without replacement. We then calculated the difference in mating proportion between each pair, and tested whether the median difference was

428 significantly different from 0 using a Wilcoxon signed rank test. The inferred biological effect
429 size was quantified by the MAP and 95% CI of the difference in mating proportion.
430
431 *Histology in wild-caught fish*
432
433 Like their relatives (79), *X. malinche* × *birchmanni* hybrids have plate-like olfactory
434 rosettes with beds of sensory epithelia surrounded by ridges of nonsensory tissue (Fig. S13).
435 Sensory epithelial beds contain a combination of ciliated and microvillous olfactory neurons,
436 which collect and transmit chemical information to the olfactory bulb, and ciliated sustentacular
437 cells, which increase flow over the beds to heighten olfactory sensitivity (80, 81). The
438 intervening nonsensory ridges are composed largely of connective tissue and goblet cells, the
439 latter of which are responsible for producing the glycoprotein-based mucus which physically
440 shields the epithelium from irritants (79, 82). Based on reports from the literature (71, 82–85),
441 we quantified the loss of cilia from the sensory epithelial surface and the proliferation of goblet
442 cells in the nonsensory epithelium and treated these two measures as a proxy for olfactory
443 disruption.
444 To understand whether polluted water was directly impacting the sensory periphery of
445 fish in *X. malinche* × *birchmanni* populations, we collected a total of 30 fish each from the
446 Aguazarca and Calnali Low populations in May (n = 10 per site) and September (n = 20) 2022.
447 Fishes were euthanized by MS-222 overdose and decapitation, after which heads were fixed in
448 10% buffered formalin for at least 48 hours. Fixed crania were dissected to remove the gills and
449 lower jaw, decalcified for 8 hours in 1X PBS with 10% formic acid, then dehydrated for 20
450 minutes each in 30%, 50%, and 70% ethanol before long-term storage in 70% ethanol. Samples

were submitted to Histo-Tec Laboratories (Hayward, CA) for xylene clearing, paraffin embedding, sectioning, and staining. Horizontal sections were taken at 5 μm intervals with a rotary microtome after removing 75–150 μm of tissue from the dorsal surface, with deeper sectioning needed to reach the olfactory epithelia in larger individuals. One slide per individual was prepared with hematoxylin and eosin (H&E) staining to observe gross morphological changes (i.e. presence/absence of ciliary on olfactory epithelium). Samples from one collection (May 2022) were also subject to Alcian Blue / Periodic Acid-Schiff stain for mucoproteins to identify mucus-producing goblet cells, with eosin as a counterstain. Individuals for whom olfactory rosettes were not present in the Histo-Tec slides (3 from Aguazarca and 1 from Calnali Low for H&E slides, 1 each for AB/PAS slides) were excluded from further analysis.

Slides were coded for blind scoring and observed at 1000X magnification using oil immersion. We defined the bounds of each sensory epithelial bed, and estimated the proportion of the surface area of each bed on which cilia were visible to the nearest 10%. Further, we scanned and imaged each slide at 40x magnification via a Biotek Cytation5 microplate reader, utilizing the in-place ruler on the image to calculate the length of each bed in ImageJ. We normalized ciliated proportions by bed length to calculate the total proportion of the sensory epithelium with visible cilia in each individual, then used a Mann-Whitney *U* test to test for differences in ciliated surface proportion between fish from Aguazarca and Calnali Low. Kolmogorov-Smirnov tests indicated that the ciliated surface proportions were not significantly different between the two sampling months ($P > 0.05$), and that other potentially confounding technical factors (number of sensory beds, individual bed length, and total bed length) also did not differ significantly between the two populations or sampling months ($P > 0.05$). To estimate the density of goblet cells, a blinded observer counted all cells positive for AB/PAS staining

within a bed, and we tested for a significant difference between populations in the number of cells per individual, corrected for total rosette length, using Mann-Whitney *U* tests. We also performed chemical treatment trials in laboratory settings to explore whether we could induce similar patterns through short-term chemical exposure (Supp. Info. 8; Fig. S14–15).

Results

Population structure across streams

Ancestry structure varied markedly among the four streams sampled for this study. One stream, the Pochula, showed a relatively smooth cline in ancestry from pure *X. malinche* at high elevations to *X. birchmanni*-like hybrids at lower elevations. The other three streams varied in the degree of population structure, with at least one site in the Calnali, Huazalingo, and Conzintla showing evidence of significant departures from unimodality based on the distribution of individual ancestry proportions (Fig. 2; Hartigan's Dip Test $P < 0.0001$). Examination of the variation in individual ancestry in these populations supported the presence of two subpopulations with distinct genome-wide ancestry.

Though we identify subpopulations of different ancestry in each stream, we infer that the drivers of these patterns differ dramatically. On the Río Huazalingo, the presence of two subpopulations was only detected at a site directly downstream of a waterfall separating pure *X. malinche* from admixed *X. birchmanni*. At this site, pure *X. malinche* individuals were sometimes detected downstream of the waterfall, but this pattern varied between sampling seasons, hinting that the *X. malinche* individuals may not persist in this population (Supp. Info. 2; Fig. S2). In the Río Conzintla, we observed sympatry between nearly-pure *X. malinche* and *X. birchmanni*; no recent-generation hybrids were detected at this site. Downstream of these sympatric sites, the *X. malinche* cluster disappears and leaves a single *X. birchmanni* ancestry cluster (Fig. 2; Table S5). The ancestry fraction in this *X. birchmanni* cluster was stable across all sites upstream of a point

where the stream passed underground (Kolmogorov-Smirnov Test $P > 0.05$), suggesting that there is little ongoing gene flow between species in this drainage.

By contrast, in the Río Calnali, we observe a dramatic collapse in population structure centered on the town of Calnali (Fig. 2). Sites upstream of the town, spanning 3.15 stream kilometers, show strong departure from unimodality in their ancestry distributions ($D = 0.12 – 0.21$, $P < 0.00001$ for all sites; Table S5). *X. malinche*-like and *X. birchmanni*-like subpopulations co-exist in sympatry across these sites, but sites downstream of the town plaza show evidence of a unimodal distribution ($D = 0.01 – 0.07$, $P > 0.18$ across all sites; Table S5) with intermediate ancestry and increased variance in individual ancestry proportion. Intriguingly, average *X. malinche* ancestry fraction increased downstream of the town of Calnali (Fig. 2), in contrast to expectations given the geographical distribution of *X. malinche* populations in other streams. To further investigate this pattern, we collected samples from tributaries flowing into this section of the Calnali, and concluded that migration of individuals with high *X. malinche* ancestry from tributaries into the main stream is a plausible explanation for this observed shift in ancestry (Supp. Info. 9; Fig. S18).

Land use across drainages

Land use quantification showed that human impact on the Río Calnali watershed was indeed higher than other streams. The reaches where the stream passed through the town of Calnali had the highest proportion of developed land in the study area, with unparalleled levels of urbanization compared to surrounding areas. This increased level of urbanization was centered on the location of genetic population structure collapse in the town of Calnali (Fig. 3). When

calculating the cumulative watershed land input of a given point, the downstream sites on the Río Calnali had the highest proportions of developed land in the study area (Fig 3B), especially when considering land within a short distance of the stream (Fig. 3E; Fig. S19H). In contrast, we observed no similar association of cleared land (vegetation, with the exclusion of forest) with population structure on the Río Calnali for any given stream reach or at the watershed scale. When compared to other streams, though, the Río Calnali did show higher levels of cumulative cleared area within a short distance of the stream (Fig. S20F, S20H). Overall, our findings suggest that disruption of forest is ubiquitous throughout the Atlapexco drainage, including in streams with low levels of hybridization. By contrast, the level of built infrastructure is especially high in the Calnali subcatchment.

Water chemistry variation aligns with breakdown of population structure

Water chemistry varied dramatically both between streams and between sites on the same stream. Principal component analysis demonstrated that the majority of variation in water quality could be summarized by two axes: one that largely separates the sites by stream (PC1), and another separating the sites upstream of the town of Calnali from the other streams and those downstream of Calnali (PC2; Fig. 4). Sites downstream of the town of Calnali were associated with increased dissolved organic matter, turbidity, ammonia, and nitrite, as well as reduced dissolved oxygen, all consistent with increased anthropogenic impacts (Fig. 4). Statistical tests indicated that levels of turbidity, DOM, nitrite, and ammonia were all significantly elevated in the sites downstream on the Río Calnali relative to the upstream sites and to other streams (Fig.

4, Supp. Fig S16; Table S7–S8). Across streams, there was variation in total conductivity, alkalinity, hardness, and pH, with sites in the Río Conzintla having the highest values of each of these metrics and sites along the Río Calnali having the lowest (Fig. 4; Fig. S22).

High concentrations of a range of metals have been previously linked to breakdowns in neurological or olfactory function in fish (28). Given the potential relationship between such breakdown and changes in ancestry assortative mating, we were interested in whether any metals were elevated in waters downstream of the town of Calnali, but not in other sites or across streams. A principal component analysis showed that concentrations of many dissolved ions, measured by ICP-MS, were highest in the Conzintla and lowest in the Calnali (Fig. 4; Fig. S24). However, the transition from the sites upstream to downstream of the town of Calnali was also associated with a dramatic increase in the concentration of numerous ions, especially major industrial metals (e.g. iron, aluminum, copper, lead, manganese; Fig. 4). Multiple metals significantly increased in concentration downstream of the town of Calnali when individually tested, including copper, lead, cadmium, aluminum, and zinc (Kruskal Wallis $P < 0.001$; Fig. 4; Fig. S23). On the other hand, other ions with known effects on fish neurobiology or olfaction showed similar or higher concentration in the Conzintla than in the Calnali downstream sites, including manganese, arsenic, and calcium (Supp. Info. 3; Fig. S24). Though we lack sufficient sampling to formally analyze these effects, we also found some evidence for temporal fluctuations in metal concentrations across streams (Supp. Info. 4; Fig. S7–9).

Finally, to quantify whether changes in water chemistry parameters were connected to land use change, we independently modelled the first two principal components of water chemistry variation as a function of both the site-wise and cumulative area of developed and cleared land, accounting for cumulative watershed area as a covariate. We found that PC1 was

strongly correlated with the cumulative area of both developed ($P < 0.001$) and cleared land ($P < 0.001$), while PC2 was associated with the proportion of developed ($P = 0.032$) and cleared ($P = 0.002$) land immediately upstream of a site. We found that limiting our analysis to land in close proximity to the stream increased the relative importance of developed land as a predictor of both PC1 and PC2. In general, our results were not sensitive to various approaches to analyzing ICP-MS values below the detection limit (Table S9–S12). We thus concluded that the proportion of built infrastructure in the watershed strongly predicted water chemistry variation, with the most dramatic impacts in the Río Calnali downstream of the town of Calnali.

Strength of ancestry-assortative mating in the Calnali Low and Aguazarca hybrid populations

In the upstream hybrid population on the Río Calnali, the Aguazarca population, we previously documented bimodal ancestry structure (56). This strong ancestry structure appears to be driven by nearly complete assortative mating by ancestry type in this population (56). By contrast, the Calnali Low population does not show evidence of bimodal ancestry structure, although variance in ancestry is high, potentially indicative of recent admixture between the *X. birchmanni* and *X. malinche* ancestry clusters (Fig. 2). We used paired mother-embryo sequencing to evaluate whether mating patterns differed from expectations under random mating with respect to ancestry. Intriguingly, despite the dramatic breakdown in population structure, we found that mothers and offspring were less different in ancestry than expected under simulations of truly random mating in both upstream and downstream populations ($P < 0.001$ by simulation; Fig. 5A). However, the difference in mother offspring ancestry was greater at Calnali Low than

591 at Calnali Mid (mean 0.0655 vs 0.0257, *t*-test $P = 0.0483$). This suggests that assortative mating
592 by ancestry is weaker in the Calnali Low hybrid population.

593 Given this result, we sought to quantify the strength of ancestry assortative mating in the
594 Calnali Low population and compare it to the upstream Calnali Mid population. We used an
595 approximate Bayesian computation approach to ask what strength of ancestry assortative mating
596 was consistent with the average difference in ancestry between mothers and offspring that we
597 observe in each hybrid population (see Methods). Based on accepted simulations, we recovered a
598 well-resolved posterior distribution of the strength of ancestry assortative mating $P_{\text{assortative}}$, and
599 estimated the maximum a posteriori (MAP) to be 0.68 (95% CI 0.20–0.82; Fig. 5B). This is
600 substantially weaker than estimates from the Calnali Mid population, in which estimates of
601 assortative mating by ancestry approach 1 (MAP = 0.97, 95% CI 0.79–0.99). A direct
602 comparison of the accepted simulations confirmed that assortative mating was significantly
603 stronger in Calnali Mid (Wilcoxon signed rank test $P < 2.2e\text{-}16$), corresponding to a MAP
604 estimated difference in the strength of assortative mating of 0.273 ($P_{\text{assortative}}$ 95% CI 0.08–0.72).
605 Thus, our results suggest that weaker assortative mating contributes to the breakdown in
606 population structure in the Calnali Low hybrid population.

607

608 *Olfactory disruption as a function of water chemistry*

609

610 Changes in olfaction can affect mate discrimination in *Xiphophorus* (24, 27), and we
611 found that fish in heavily impacted sites on the Río Calnali have been exposed to high levels of a
612 range of compounds that may impact olfactory function. We therefore evaluated evidence for
613 physical damage of the olfactory rosettes of wild caught fish from different sites on the Río

614 Calnali, and found that fish collected from the upstream site, Aguazarca, and the downstream
615 site, Calnali Low, showed significant changes in olfactory morphology. H&E staining allowed us
616 to observe the motile and sensory cilia which may be lost in the face of chemical exposure (71,
617 83, 84). We found marginally lower proportions of ciliated surface area on the olfactory
618 epithelium at the Calnali Low site (Mann-Whitney Test $P = 0.08$; Fig. 5C). Likewise, AB/PAS
619 staining clearly distinguished goblet cells through the deep blue staining of the protective
620 mucoproteins they produce, and revealed significantly higher densities of goblet cells at Calnali
621 Low (Mann-Whitney Test $P = 0.003$; Fig. 5D–F), consistent with a compensatory response to
622 shield the olfactory epithelium from toxicants.

Discussion

With a fine-scale view of the genetic and environmental landscape of hybrid zones, we can move past a binary picture of hybridization's occurrence to assess the specific changes and mechanisms driving anthropogenic hybridization. By surveying genome-wide ancestry distributions from thousands of samples across dozens of sites where *X. birchmanni* and *X. malinche* coexist, we found that the patterns of hybridization varied drastically within and between streams. We detected some degree of gene flow between *X. malinche* and *X. birchmanni* in all four streams surveyed, but the amount and spatial distribution of admixture differed across each stream (Fig. 2, Supp. Info. 9; Fig. S16–17). Thus, while there is some potential for hybridization whenever related species overlap, the implications for evolution are highly variable.

At one end of the spectrum of genetic homogenization, the Río Conzintla showed two slightly admixed ancestry clusters which co-occur at multiple sites across 3.7 stream kilometers, resulting in a bimodal distribution of genome-wide ancestry at these sites. Within these sites, individuals derived <15% of their genome-wide ancestry from the other species (mean ± SD minor parent ancestry of 5.6 ± 3.1% at Xochicoatlán, 10.6 ± 4.5% at Mixtla). While this level of admixture is evolutionarily significant, its functional consequences may be limited by genome-wide selection against introgression (50), and populations with similar admixture rates have been designated as "conservation populations" in other cases of anthropogenic hybridization (86). The stability of within-cluster admixture proportions across the entire length of the Río Conzintla, combined with our observation of only 1 recent hybrid out of 239 individuals, suggests that gene flow between clusters in this stream is extremely limited. The stable hybrid zone in this stream

646 thus serves as a contrast to other streams, and comparisons in water quality may illuminate the
647 potential drivers of breakdown in assortative mating in other contexts.

648 In contrast, the Huazalingo and Pochula streams showed no sites with bimodal ancestry
649 structure, but rather a sharp transition in genome-wide ancestry moving downstream. These
650 streams appear more similar to classic clinal hybrid zones, where ancestry patterns are shaped by
651 the countervailing effects of gene flow and selection against hybrids (87). While the lack of any
652 structured populations in these streams prevented us from assessing the effects of environmental
653 variation on rates of hybridization, we found that overall water chemistry in these streams was
654 quite similar to the Río Conzintla. We speculate that past anthropogenic impacts could have
655 played a role in the onset of hybridization in these streams, but it is difficult to test such
656 hypotheses in contemporary hybrid populations, since the weakening of mate preference in
657 admixed individuals means that hybridization can continue even after environmental triggers
658 disappear (88–90). These streams nonetheless can provide important insights into the role of
659 migration and ecological selection in structuring *X. malinche* × *X. birchmanni* hybrid zones
660 (Supp. Info. 9).

661 Lastly, the Río Calnali showed a dramatic change in ancestry structure from upstream to
662 downstream. We observed strong bimodality in genome-wide ancestry at sites upstream of the
663 town of Calnali, with individuals falling into one of two subpopulations, a *X. malinche*-like
664 ancestry cluster and a *X. birchmanni*-like cluster. These results align with prior work
665 documenting the presence of strong assortative mating by ancestry within *X. malinche* and *X.*
666 *birchmanni*-like hybrid clusters at the Aguazarca site on the Río Calnali (Supp. Info. 6) (56).
667 Within a span of less than two stream kilometers where the stream traverses the town of Calnali,
668 this bimodal population structure collapses into a hybrid swarm, with the range of observed

admixture proportions spanning the continuum between the upstream clusters (Fig. 2). The Río Calnali thus provides a powerful opportunity to study the environmental determinants of reproductive isolation through comparisons within and between streams.

We took advantage of this remarkable system by measuring a large array of chemical parameters in parallel with our genomic surveys across streams. In doing so, we identified substantial chemical variation both between streams and between sites upstream and downstream of the town of Calnali (Fig. 4). PCA highlighted stream-specific water chemistry signatures, which we speculate may be driven by geology and the impacts of mining in the Conzintla drainage (see Supp. Info. 3; Fig. S5). However, we also observe an orthogonal chemical change among sites on the Río Calnali above and below the town of Calnali, while the other streams were relatively stable in water chemistry along their lengths (Fig. 4). By quantifying land use across each drainage, we confirmed that the Calnali drainage is unique both in the scale of built infrastructure relative to catchment area, as well as the proximity of development to the stream (Fig. 3, Fig. S19). The clearing of forests for pasture and cropland could also contribute to the chemical disturbances we observe, but may be a less likely explanation given the relatively small differences in agricultural land areas within and between drainages (Fig. S20), as well as the low-intensity agricultural practices typical of the region (91, 92). Both agricultural and urban development have been linked to some of the changes in water chemistry that we observe in the downstream Río Calnali (93–97). In particular, many metals whose concentrations change along the course of the Río Calnali have been previously associated with both domestic wastewater and runoff from roads (95).

Among the many compounds which varied between streams and disturbance regimes, a substantial number have been previously shown to affect olfaction in fishes (dissolved organic

matter, copper, aluminum, zinc (24, 98, 99)) or fish neurology more generally (ammonia, cobalt, and cadmium (69, 75, 100)). Many of these parameters were specifically elevated in the Río Calnali, and especially so in the areas downstream of the town. Thus, they are particularly promising candidates for the drivers of ancestry structure breakdown. On the other hand, we found that other ions with olfactory or neurological effects in the ecotoxicology literature (manganese, arsenic, calcium (27, 101–103)) were most extreme in the Conzintla, where reproductive isolation is maintained (Fig. S22, Fig. S24), suggesting that variation in these specific parameters is not a primary driver of hybridization in *Xiphophorus*. Variation in pH between streams may also play a role, as low pH increases metal bioavailability (Fig. S22; (98)).

Having established differences in both the degree of population structure and in water chemistry between sites in the Río Calnali, we next explored the loss of olfaction-based assortative mate preferences as a biological mechanism which might connect the two. Mother-embryo sequencing and simulations demonstrate that assortative mating is substantially weakened at downstream sites on the Río Calnali, but surprisingly, it is not entirely absent (Fig. 5B). Ongoing assortative mating could be driven by downstream migration, with mothers either mating prior to migration, or retaining some ability to mate assortatively even after arriving in highly polluted waters. Alternatively, weak assortative mating at the population scale could be produced by different impacts of pollution on different sensory pathways used in mate choice (e.g. visual vs. olfactory cues, (104, 105)) or fluctuations in the degree of sensory disturbance fish experience as a result of variation in environmental conditions (Supp. Info. 4). Regardless of the precise drivers, our findings support theoretical predictions that even modest reductions in the strength of assortative mating may result in the emergence of hybrid swarms (30).

714 Finally, our histological sampling of fishes in the upstream and downstream Calnali shows
715 changes in cellular abundance and morphology consistent with olfactory damage. The loss of
716 cilia in the sensory epithelium has previously been observed after exposure to heavy metals and
717 anthropogenic hydrocarbons (80, 106), and could directly reduce olfactory sensitivity by
718 disrupting water flow through the nares (107, 108) or the function of olfactory sensory neurons
719 (109). Likewise, an increased number of goblet cells has been linked to inflammation secondary
720 to nasal irritation in other systems, and may protect epithelial tissue from noxious chemical
721 exposure (82, 85). These histological analyses represent the first evidence of more severe
722 olfactory damage in a wild hybrid swarm relative to nearby structured populations. Whether
723 these changes themselves weaken assortative mating, or are correlated with other causative
724 changes (e.g. transport and accumulation of heavy metals in the brain's olfactory bulb (110)) is
725 an exciting direction for future work. While our results support the hypothesis that the
726 breakdown of assortative mating along the Río Calnali is mediated at least in part by olfactory
727 dysfunction, our short-term laboratory exposures of *X. birchmanni* to ecologically relevant levels
728 of ammonia, copper, humic acid, or their combination did not reproduce the effect (Fig. S15).
729 This suggests that the damage we observe in wild populations may be a result of long-term
730 exposure, or the more complex repertoire of compounds individuals are exposed to in natural
731 populations.
732 Taken as a whole, our study presents an integrative window into the environmental and
733 organismal drivers of hybridization between *X. birchmanni* and *X. malinche*. By showing that
734 dramatic water chemistry differences are tightly linked to changes in population structure, we
735 confirm the relevance of prior behavioral work showing the potential for changes in water
736 chemistry to disrupt assortative mating in these species (24, 27). Though many studies have

documented a broad connection between environmental conditions and hybridization in freshwater fishes (5, 28), our analyses of assortative mating and olfactory histology provide a deeper understanding of the proximal mechanisms by which water chemistry changes might disrupt reproductive isolation on small spatiotemporal scales. As human impacts on the environment continue to expand, a greater understanding of the drivers of hybridization will help to mitigate human impacts on biodiversity, and will continue to deepen our understanding of the speciation process.

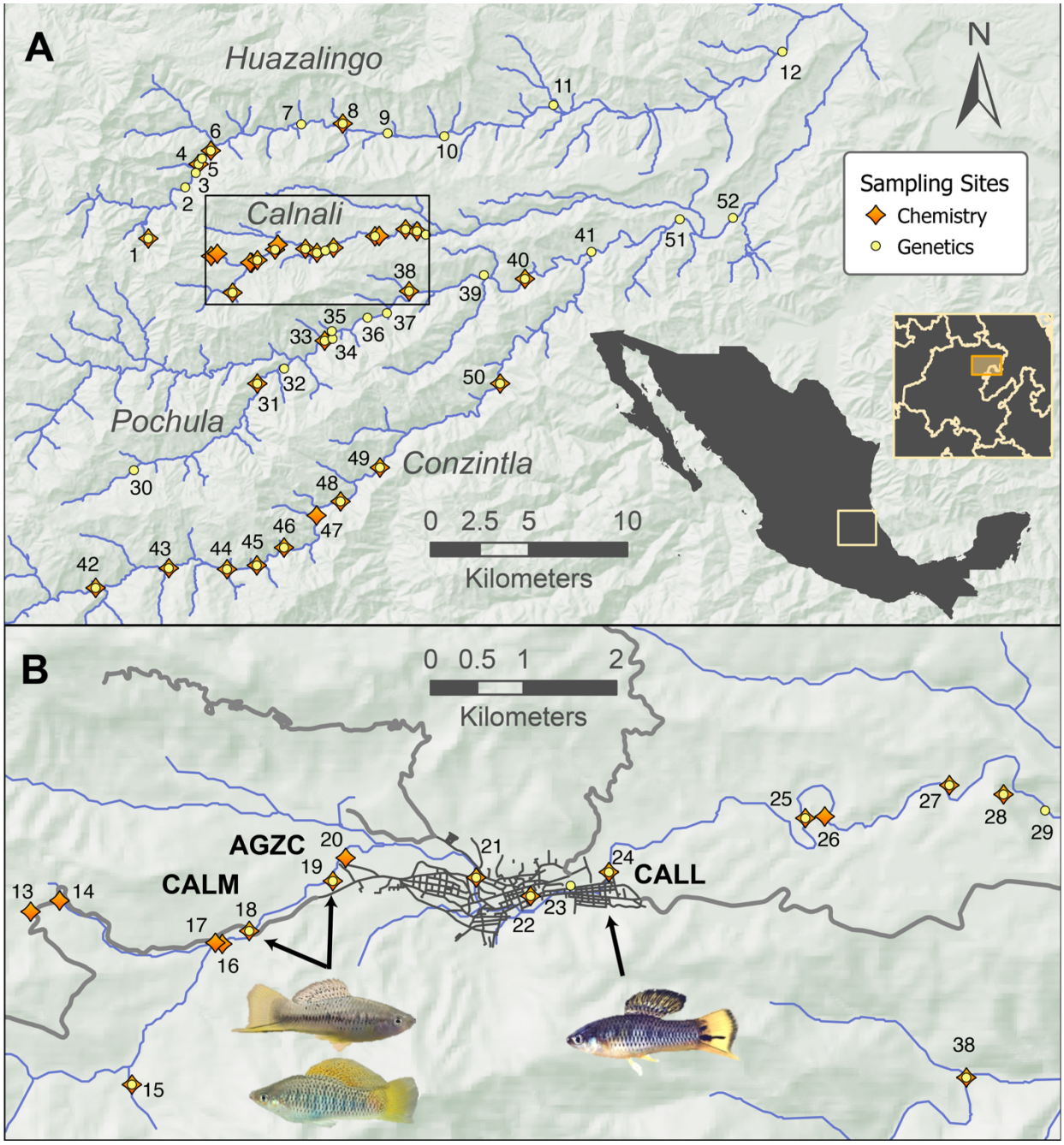

Figure 1. Study area and sampling sites. **A)** Overview of Río Atlapexco basin, highlighted in orange within the inset Mexican state map, whose area is indicated in yellow on the gray outline of Mexico. Streams are shown as blue lines, the four major streams studied are labelled, sites where fish were collected are yellow circles, and sites where water chemistry data were collected are orange diamonds. The black box encloses the area displayed in panel **B**. **B)** Sites sampled on

Río Calnali. Thick gray lines show major roadways, and thin black lines show streets in the town of Calnali. Images show representative male *Xiphophorus* fishes with *X. malinche*-like (top left), *X. birchmanni*-like (bottom left) and admixed (right) phenotypes as observed in three populations on the Río Calnali (AGZC = Aguazarca, CALM = Calnali Mid, CALL = Calnali Low). These sites were also the locations used for sample collection for mother-embryo sequencing (CALM and CALL) and histology (AGZC and CALL). In the Río Calnali, *X. malinche*-like fish are found in the headwaters, *X. malinche*-like and *X. birchmanni*-like fishes are found upstream of the town of Calnali, and fish with intermediate genotypes and phenotypes are found downstream of town.

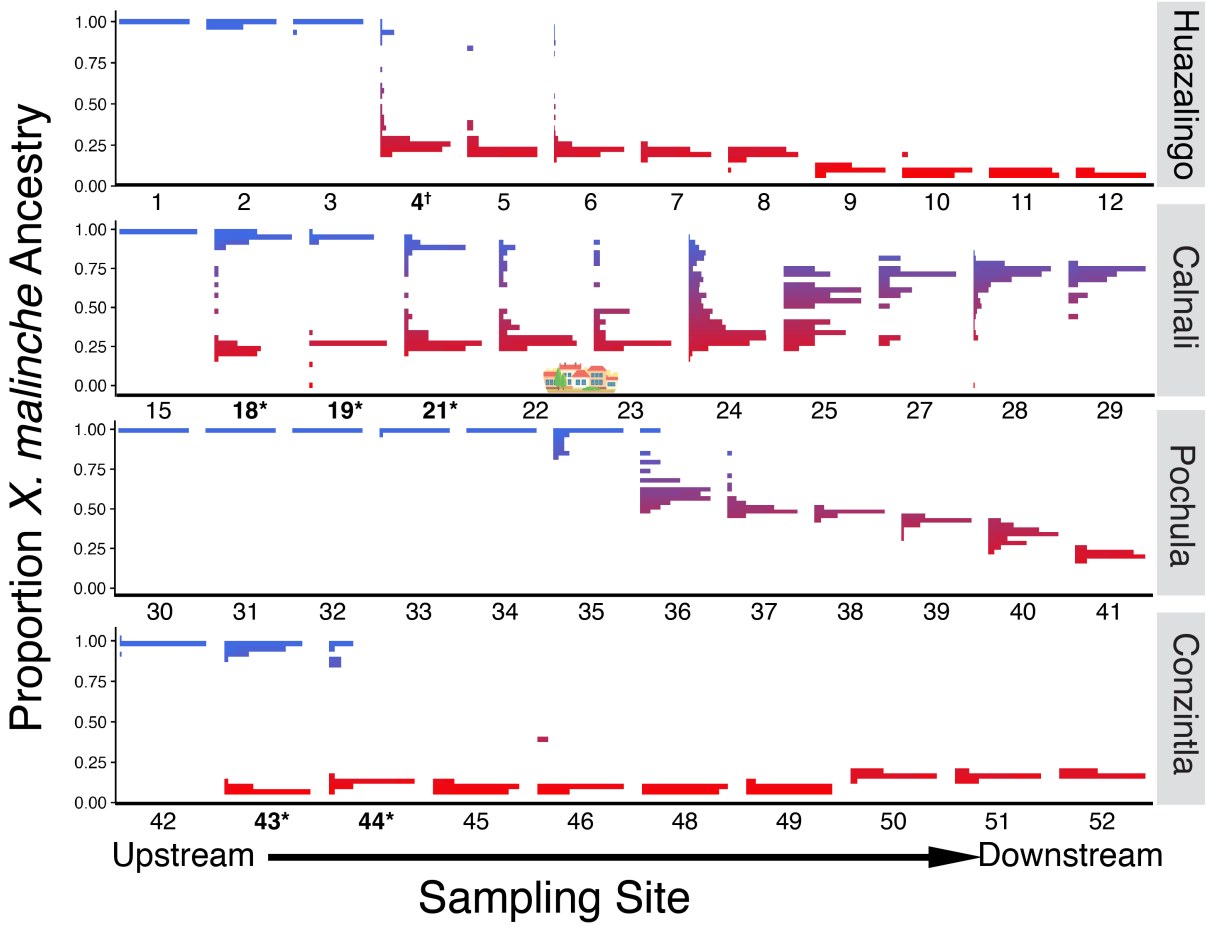

Figure 2. Genetic ancestry results from *X. malinche* × *X. birchmanni* hybrids in the Río Atlapexco Drainage. Histograms show ancestry distributions at sampling locations along four streams in the Río Atlapexco drainage. Sites are arranged with upstream sites on the left side of the X-axis, and downstream sites on the right. Y-axis corresponds to the proportion of genome-wide ancestry derived from *X. malinche* among individuals in that populations (1 = pure *X. malinche*, 0 = pure *X. birchmanni*), and the width of bars indicates the frequency of individuals in that ancestry bin. Building icon on the Río Calnali transect denotes the sites located within the town of Calnali. X-axis text shows site numbers, as in Fig. 1. Bolded X-axis numbers indicate sites with significant deviations from a unimodal ancestry distribution, either across all sampling timepoints (asterisk) or at a subset of sampling times (dagger, Supp. Info. 2).

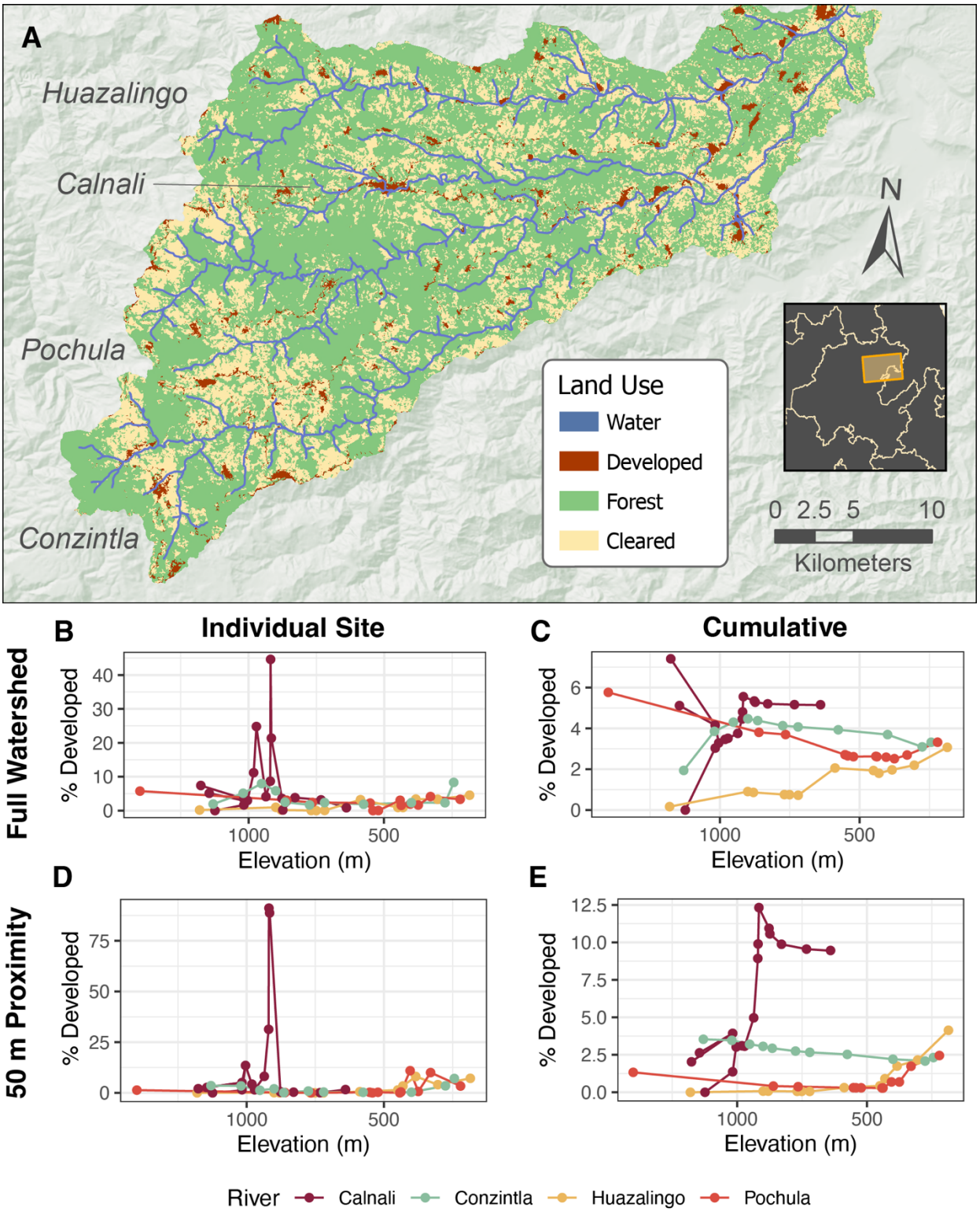

Figure 3. Results of land use classification analysis in the Río Atlapexco basin. **A**) Map of classification results from 2020–2023 hyperspectral imagery. 10 m^2 pixels were classified as

developed (buildings, mines, and roads), cleared land (grassland, pasture, or cultivated crops) forest (continuous tree cover, excluding plantation-style agriculture), or water by an SVM algorithm, with training polygons identified from 3 m^2-resolution 2022 imagery from Planet Labs (62). Stream polygons are shown as blue lines over classified pixels. **B–E)** Percent of land classified as developed within different drainages of the Río Atlapexco basin. Points show the proportion of pixels in each site's subcatchment that were classified as developed. Left column (**B** and **D**) shows the site-wise proportions, or the subcatchment of the section of stream between a site and the closest upstream site. Right column (**C** and **E**) shows the cumulative subcatchment of all sections of the stream upstream of a given site. Top row (**B** and **C**) shows calculations that include pixels of any distance from a stream, while bottom row (**D** and **E**) shows calculations limited to pixels within 50 m of a stream (defined as pixels with accumulated flow > 3000 cells, depicted with stream polygons in **A**). Color denotes the drainage that the site occurs in, and lines connect sites in the same stream based on their order. The line corresponding to the Río Calnali branches because multiple headwater tributaries were sampled.

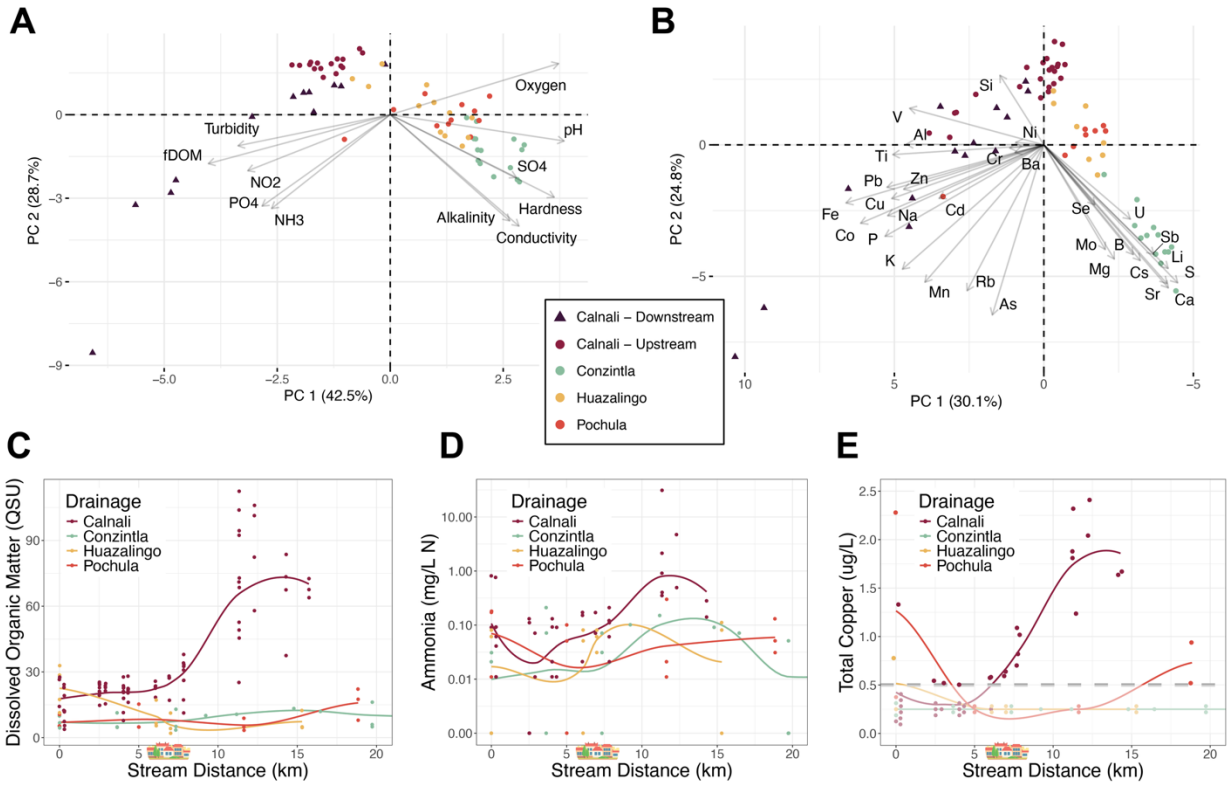

Figure 4. Water chemistry data from four streams in the Río Atlapexco drainage. **A–B)** Principal component analysis (PCA) biplot for **A)** parameters measured using the sonde, turbidimeter, colorimeter, and **B)** parameters measured using ICP-MS. Points represent sampling events, and color and shape denote drainage, with sites on the Río Calnali upstream and downstream of the town of Calnali labelled separately. Labelled arrows represent variable loadings onto first two principal components, with highly correlated variables showing similar vectors. **C–E)** Plots of the change in water chemistry over the course of the stream, focusing on parameters that were elevated in sites downstream of the town of Calnali. These include **C)** fluorescent dissolved organic matter, **D)** ammonia, and **E)** total copper. The building icon on the X-axis denotes the sites located within the town of Calnali on the Río Calnali transect. X-axis indicates distance downstream from the first site sampled on a stream, points indicate individual measurements, and lines show a loess-spline fit of change over the stream course. Note that the Y-axis is log-

scaled in the case of ammonia measurements (**D**). Translucent points below the gray dashed line in **E)** represent measured values below the detection limit of the ICP-MS assay. Points below this limit are plotted at half the detection threshold, with jittering to prevent overlap and represent sample size, but do not represent point estimates of the concentration.

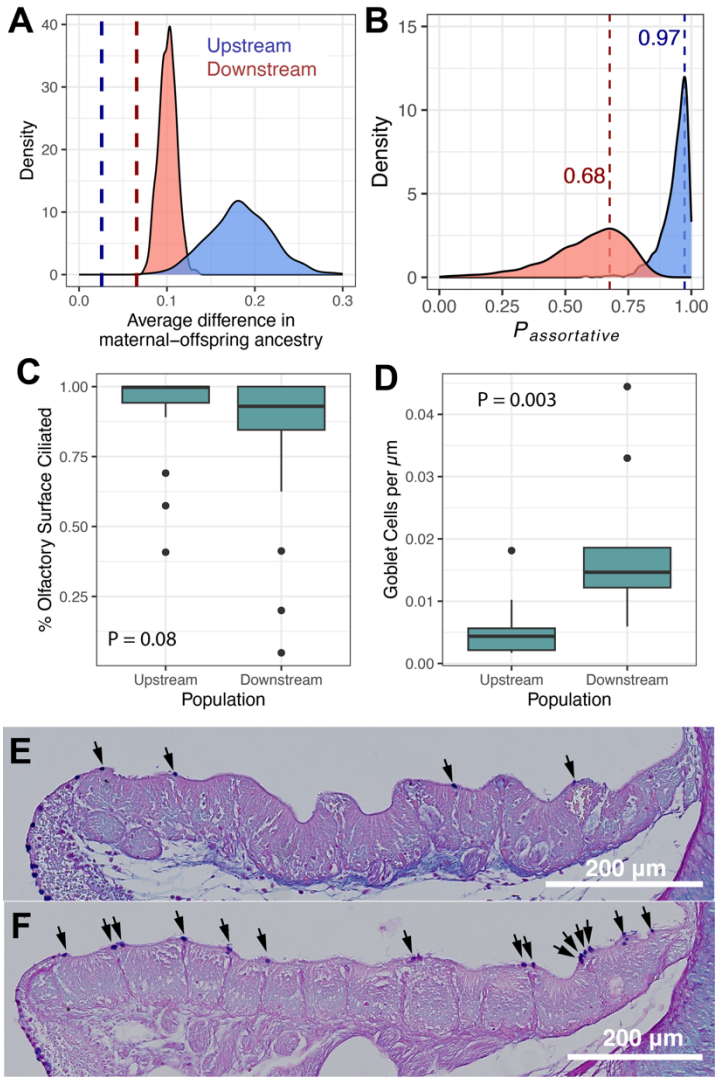

Figure 5. Mating patterns and histological phenotypes in fishes upstream and downstream of the town of Calnali. **A)** Results of mother-embryo sequencing analysis based on individuals collected at sites downstream (Calnali Low, red) and upstream (Calnali Mid, blue) of the town of Calnali. Density curves show the distribution of average mother-embryo ancestry difference across 1000 simulations of random mating in each population, and dashed lines show the observed average mother-embryo ancestry difference based on our data. Mean maternal-offspring ancestry difference was significantly lower than expected under random mating for both populations, consistent with assortative mating by ancestry ($P < 0.001$). **B)** Inferred strength

813 of assortative mating from observed maternal-offspring ancestry distributions. Density curves
814 depict the simulated probability of assortative mating ($P_{assortative}$) in accepted simulations for each
815 population, with 0 representing random mating. Dashed line denotes maximum a posteriori
816 estimates (Calnali Low = 0.68, Calnali Mid = 0.97). **C–D)** Results of olfactory histology of
817 fishes from sites upstream (Aguazarca) and downstream (Calnali Low) of the town of Calnali. **C)**
818 Proportion of each fish's sensory epithelium with visible cilia, visualized with H&E staining. **D)**
819 Number of mucus-producing goblet cells per µm of olfactory rosette surface area, visualized by
820 staining with AB/PAS. *P*-values indicate results of Mann-Whitney *U* Test for difference between
821 sites. **E–F)** Representative AB/PAS stains of olfactory rosettes of *X. malinche* × *birchmanni*
822 hybrids from **E)** Aguazarca, and **F)** Calnali Low. Mucoproteins are stained blue by AB/PAS,
823 eosin counterstain appears as pink. Arrowheads indicate locations of goblet cells, with the inset
824 pictures from individuals exhibiting the median count for each population.

Acknowledgements

The authors thank members of the Schumer and Rosenthal laboratories for helpful discussion and/or feedback on earlier versions of this manuscript. We thank the Federal Government of Mexico for permission to collect fish (Permiso de Pesca de Fomento no. PPF/DGOPA-064/20). Stanford University and the Stanford Research Computing Center provided computational support for this project. We thank Dra. Susana Saval Bohórquez of the UNAM Environmental Engineering Laboratory and Dr. Guangchao Li and Douglas Turner of the Stanford Environmental Measurements Facility for technical and experimental support. We are deeply grateful to the delegates and landowners of the Calnali region for their engagement in our work and for sharing access to their communities' waterways. This work was supported by a Knight–Hennessy Scholars fellowship and NSF GRFP 2019273798 to B.M.M., a CONACyT fellowship to GIJ, NSF Awards 1723266, 1755327 and 1354172 to GGR, and Human Frontiers in Science Grant RGY0081 to MS & CMR. The authors declare no conflicts of interest related to this work.

Data Availability

Raw sequencing reads used in this project are available under NCBI SRA Bioprojects PRJNAXXXXXX (accession pending). All other datasets necessary to recreate the results of the publication are available on Dryad (accession pending). All new customs scripts used to generate results are available on Github at https://github.com/Schumerlab/anthro_xipho_hybrids and https://github.com/Schumerlab/Lab_shared_scripts.

References

1. R. J. Abbott, N. H. Barton, J. M. Good, Genomics of hybridization and its evolutionary consequences. *Molecular Ecology* **25**, 2325–2332 (2016).

2. N. H. Barton, The role of hybridization in evolution. *Molecular Ecology* **10**, 551–568 (2001).

3. E. Mayr, *Systematics and the Origin of Species: from the Viewpoint of a Zoologist* (Columbia University Press, 1942).

4. E. Anderson, Hybridization of the habitat. *Evolution* 1–9 (1948).

5. K. C. Grabenstein, S. A. Taylor, Breaking Barriers: Causes, Consequences, and Experimental Utility of Human-Mediated Hybridization. *Trends in Ecology & Evolution* **33**, 198–212 (2018).

6. J.-G. J. Godin, S. E. Briggs, Female mate choice under predation risk in the guppy. *Animal Behaviour* **51**, 117–130 (1996).

7. P. M. Willis, M. J. Ryan, G. G. Rosenthal, Encounter rates with conspecific males influence female mate choice in a naturally hybridizing fish. *Behavioral Ecology* **22**, 1234–1240 (2011).

8. M. N. Verzijden, Z. W. Culumber, G. G. Rosenthal, Opposite effects of learning cause asymmetric mate preferences in hybridizing species. *Behavioral Ecology* **23**, 1133–1139 (2012).

9. J. Hunt, R. Brooks, M. D. Jennions, Female Mate Choice as a Condition-Dependent Life-History Trait. *The American Naturalist* **166**, 79–92 (2005).

10. A. E. Hausmann, *et al.*, Light environment influences mating behaviours during the early stages of divergence in tropical butterflies. *Proceedings of the Royal Society B: Biological Sciences* **288**, 20210157 (2021).

11. K. S. Pfennig, Facultative mate choice drives adaptive hybridization. *Science* **318**, 965–967 (2007).

12. G. G. Rosenthal, D. Stuart-Fox, others, "Environmental disturbance and animal communication" in *Behavioural Responses to a Changing World: Mechanisms and Consequences*, (Oxford University Press, 2015), pp. 16–31.

13. G. G. Rosenthal, Individual mating decisions and hybridization. *Journal of Evolutionary Biology* **26**, 252–255 (2013).

14. O. Seehausen, J. J. M. van Alphen, F. Witte, Cichlid Fish Diversity Threatened by Eutrophication That Curbs Sexual Selection. *Science* **277**, 1808–1811 (1997).

15. B. Seifert, J. Kulmuni, P. Pamilo, Independent hybrid populations of Formica polyctena Xrufa wood ants (Hymenoptera: Formicidae) abound under conditions of forest fragmentation. *Evol Ecol* **24**, 1219–1237 (2010).

16. J. A. Coyne, H. A. Orr, *Speciation* (Sinauer Associates, 2004).

17. D. A. Turissini, J. A. McGirr, S. S. Patel, J. R. David, D. R. Matute, The Rate of Evolution of Postmating-Prezygotic Reproductive Isolation in Drosophila. *Molecular Biology and Evolution* **35**, 312–334 (2018).

18. D. I. Bolnick, T. J. Near, Tempo of Hybrid Inviability in Centrarchid Fishes (TELeostei: Centrarchidae). *Evolution* **59**, 1754–1767 (2005).

19. C. E. Wagner, L. J. Harmon, O. Seehausen, Ecological opportunity and sexual selection together predict adaptive radiation. *Nature* **487**, 366–369 (2012).

20. O. Puebla, E. Bermingham, F. Guichard, Pairing dynamics and the origin of species. *Proceedings of the Royal Society of London B: Biological Sciences* **279**, 1085–1092 (2012).

21. R. Ubsdell, Studies on variation and evolution in Centaurium erythraea Rafn and C. littorale (D. Turner) Gilmour in the British Isles. 3. Breeding systems, floral biology and general discussion. *Watsonia* **12**, 225–232 (1979).

22. C. Brochmann, Hybridization and distribution of Argyranthemum coronopifolium (Asteraceae – Anthemideae) in the Canary Islands. *Nordic Journal of Botany* **4**, 729–736 (1984).

23. P. Vonlanthen, *et al.*, Eutrophication causes speciation reversal in whitefish adaptive radiations. *Nature* **482**, 357–362 (2012).

24. H. S. Fisher, B. B. M. Wong, G. G. Rosenthal, Alteration of the chemical environment disrupts communication in a freshwater fish. *Proc R Soc B* **273**, 1187–1193 (2006).

25. J. L. Ward, M. J. Blum, Exposure to an environmental estrogen breaks down sexual isolation between native and invasive species. *Evolutionary Applications* **5**, 901–912 (2012).

26. P. C. Hubbard, E. N. Barata, A. V. M. Canario, Possible disruption of pheromonal communication by humic acid in the goldfish, Carassius auratus. *Aquatic Toxicology* **60**, 169–183 (2002).

27. D. L. Powell, A. D. Rose, G. G. Rosenthal, A widely-used pollutant causes reversal of conspecific mate preference in a freshwater fish. [Preprint] (2022). Available at: https://www.biorxiv.org/content/10.1101/2022.09.07.507014v1 [Accessed 2 September 2023].

28. W. F. Ramirez-Duarte, *et al.*, Hybridization in the Anthropocene – how pollution and climate change disrupt mate selection in freshwater fish. *Biological Reviews* **0** (2024).

29. E. C. Ellis, Anthropogenic transformation of the terrestrial biosphere. *Philosophical Transactions of the Royal Society A: Mathematical, Physical and Engineering Sciences* **369**, 1010–1035 (2011).

30. R. T. Gilman, J. E. Behm, Hybridization, Species Collapse, and Species Reemergence After Disturbance to Premating Mechanisms of Reproductive Isolation. *Evolution* **65**, 2592–2605 (2011).

31. D. J. Hasselman, *et al.*, Human disturbance causes the formation of a hybrid swarm between two naturally sympatric fish species. *Molecular Ecology* **23**, 1137–1152 (2014).

32. T. B. Malek, J. W. Boughman, I. Dworkin, C. L. Peichel, Admixture mapping of male nuptial colour and body shape in a recently formed hybrid population of threespine stickleback. *Molecular Ecology* **21**, 5265–5279 (2012).

33. B. Alric, *et al.*, Local human pressures influence gene flow in a hybridizing Daphnia species complex. *Journal of Evolutionary Biology* **29**, 720–735 (2016).

34. T. van Hengstum, *et al.*, Human-induced hybridization among congeneric endemic plants on Tenerife, Canary Islands. *Plant Syst Evol* **298**, 1119–1131 (2012).

35. J. I. Meier, *et al.*, Ancient hybridization fuels rapid cichlid fish adaptive radiations. *Nature Communications* **8**, 14363 (2017).

36. S. A. Taylor, E. L. Larson, Insights from genomes into the evolutionary importance and prevalence of hybridization in nature. *Nat Ecol Evol* **3**, 170–177 (2019).

37. M. Schumer, R. Cui, G. G. Rosenthal, P. Andolfatto, Reproductive Isolation of Hybrid Populations Driven by Genetic Incompatibilities. *PLoS Genet* **11**, e1005041 (2015).

38. C. Veller, N. B. Edelman, P. Muralidhar, M. A. Nowak, Recombination and selection against introgressed DNA. *Evolution* **77**, 1131–1144 (2023).

39. C. Chen, K. S. Pfennig, Female toads engaging in adaptive hybridization prefer high-quality heterospecifics as mates. *Science* **367**, 1377–1379 (2020).

40. N. B. Edelman, J. Mallet, Prevalence and Adaptive Impact of Introgression. *Annu Rev Genet* **55**, 265–283 (2021).

41. M. Ribeiro Palacios, Land use change in Southern Huasteca, Mexico; drivers and consequences for livelihood and ecosystem services. (2012).

42. H. R. Hernández, M. A. Robledo, J. R. A. Rivera, J. F. Martinez, Spatial Configuration of Land-Use/Land-Cover in the Pujal-Coy Project Area, Huasteca Potosina Region, Mexico. *Ambio* **37**, 381–389 (2008).

43. M. L. Martínez, *et al.*, Effects of land use change on biodiversity and ecosystem services in tropical montane cloud forests of Mexico. *Forest Ecology and management* **258**, 1856–1863 (2009).

44. L. Chapa-Vargas, K. Monzalvo-Santos, Natural protected areas of San Luis Potosí, Mexico: ecological representativeness, risks, and conservation implications across scales. *International Journal of Geographical Information Science* **26**, 1625–1641 (2012).

45. C. Payne, *et al.*, Genomic insights into variation in thermotolerance between hybridizing swordtail fishes. *Mol Ecol* (2022). https://doi.org/10.1111/mec.16489.

46. Z. W. Culumber, D. B. Shepard, S. W. Coleman, G. G. Rosenthal, M. Tobler, Physiological adaptation along environmental gradients and replicated hybrid zone structure in swordtails (Teleostei: Xiphophorus). *Journal of Evolutionary Biology* **25**, 1800–1814 (2012).

47. D. L. Powell, *et al.*, Natural hybridization reveals incompatible alleles that cause melanoma in swordtail fish. *Science* **368**, 731–736 (2020).

48. B. M. Moran, *et al.*, A lethal mitonuclear incompatibility in complex I of natural hybrids. *Nature* **626**, 119–127 (2024).

49. M. Schumer, Y. Brandvain, Determining epistatic selection in admixed populations. *Mol Ecol* **25**, 2577–2591 (2016).

50. M. Schumer, *et al.*, Natural selection interacts with recombination to shape the evolution of hybrid genomes. *Science* **360**, 656–660 (2018).

51. Z. W. Culumber, *et al.*, Replicated hybrid zones of *Xiphophorus* swordtails along an elevational gradient. *Mol Ecol* **20**, 342–356 (2011).

52. M. Rauchenberger, I. K. D. Kallman, Monophyly and Geography of the Rio P'anuco Basin Swordtails (Genus Xiphophorus) with Descriptions of Four New Species. *AMERICAN MUSEUM NOVITATES* 44 (1990).

53. G. G. Rosenthal, *et al.*, Dissolution of Sexual Signal Complexes in a Hybrid Zone between the Swordtails Xiphophorus birchmanni and Xiphophorus malinche (Poeciliidae). *Copeia* **2003**, 299–307 (2003).

54. INEGI, México en cifras. (1998). Available at: https://www.inegi.org.mx/app/areasgeograficas/ [Accessed 7 April 2025].

55. M. Schumer, *et al.*, High-resolution mapping reveals hundreds of genetic incompatibilities in hybridizing fish species. *eLife* **3**, e02535 (2014).

56. M. Schumer, *et al.*, Assortative mating and persistent reproductive isolation in hybrids. *Proc Natl Acad Sci USA* **114**, 10936–10941 (2017).

57. M. Schumer, D. L. Powell, R. Corbett-Detig, Versatile simulations of admixture and accurate local ancestry inference with mixnmatch and ancestryinfer. *Molecular Ecology Resources* **20**, 1141–1151 (2020).

58. S. M. Banerjee, *et al.*, Complex hybridization between deeply diverged fish species in a disturbed ecosystem. *Evolution* **77**, 995–1005 (2023).

59. J. A. Hartigan, P. M. Hartigan, The Dip Test of Unimodality. *The Annals of Statistics* **13**, 70–84 (1985).

60. European Union/ESA/Copernicus, Sentinel-2 MSI: MultiSpectral Instrument, Level-2A. (2020).

61. J. Transon, R. D'Andrimont, A. Maugnard, P. Defourny, Survey of Hyperspectral Earth Observation Applications from Space in the Sentinel-2 Context. *Remote Sensing* **10**, 157 (2018).

62. Planet Labs, Planetscope Scene, March 29 2022, Instrument PS2.SD, Strip 5529184. (2022).

63. INEGI, Continuo de elevaciones mexicano y modelos digitales de elevación v3. (2013).

64. A. Kamal, K. Wichuk, D. McCartney, K. Londry, C. Felske, Effect of Treated Wood on Biosolids Composting. *Compost Science & Utilization* **25**, 178–193 (2017).

65. K. J. Pieper, *et al.*, Evaluating Water Lead Levels During the Flint Water Crisis. *Environ. Sci. Technol.* **52**, 8124–8132 (2018).

66. D. R. Helsel, *Nondetects and data analysis. Statistics for censored environmental data.* (2005).

67. O. Seehausen, *et al.*, Speciation through sensory drive in cichlid fish. *Nature* **455**, 620–626 (2008).

68. J.-H. Kim, S. K. Kim, Y. B. Hur, Toxic effects of waterborne nitrite exposure on antioxidant responses, acetylcholinesterase inhibition, and immune responses in olive flounders, *Paralichthys olivaceus*, reared in bio-floc and seawater. *Fish & Shellfish Immunology* **97**, 581–586 (2020).

69. Y. K. Ip, S. F. Chew, D. J. Randall, "Ammonia toxicity, tolerance, and excretion" in *Fish Physiology*, Nitrogen Excretion., (Academic Press, 2001), pp. 109–148.

70. D. J. Randall, T. K. N. Tsui, Ammonia toxicity in fish. *Marine Pollution Bulletin* **45**, 17–23 (2002).

71. J. A. Hansen, J. D. Rose, R. A. Jenkins, K. G. Gerow, H. L. Bergman, Chinook salmon (Oncorhynchus tshawytscha) and rainbow trout (Oncorhynchus mykiss) exposed to copper: Neurophysiological and histological effects on the olfactory system. *Environmental Toxicology and Chemistry* **18**, 1979–1991 (1999).

1013 72. W. A. Dew, A. Azizishirazi, G. G. Pyle, Contaminant-specific targeting of olfactory sensory
1014 neuron classes: Connecting neuron class impairment with behavioural deficits.
1015 *Chemosphere* **112**, 519–525 (2014).

1016 73. J.-W. Lee, *et al.*, Toxic effects of lead exposure on bioaccumulation, oxidative stress,
1017 neurotoxicity, and immune responses in fish: A review. *Environmental Toxicology and*
1018 *Pharmacology* **68**, 101–108 (2019).

1019 74. C. R. Williams, E. P. Gallagher, Effects of cadmium on olfactory mediated behaviors and
1020 molecular biomarkers in coho salmon (Oncorhynchus kisutch). *Aquatic Toxicology* **140–**
1021 **141**, 295–302 (2013).

1022 75. K. Heffern, K. Tierney, E. P. Gallagher, Comparative effects of cadmium, zinc, arsenic and
1023 chromium on olfactory-mediated neurobehavior and gene expression in larval zebrafish
1024 (*Danio rerio*). *Aquatic Toxicology* **201**, 83–90 (2018).

1025 76. J. T. Hentig, C. A. Byrd-Jacobs, Exposure to zinc sulfate results in differential effects on
1026 olfactory sensory neuron subtypes in adult zebrafish. *International journal of molecular*
1027 *sciences* **17**, 1445 (2016).

1028 77. D. A. Klaprat, S. Brown, T. J. Hara, The effect of low pH and aluminum on the olfactory
1029 organ of rainbow trout, Salmo gairdneri. *Environmental Biology of Fishes* **22**, 69–77
1030 (1988).

1031 78. K. A. Paczolt, *et al.*, Multiple Mating and Reproductive Skew in Parental and Introgressed
1032 Females of the Live-Bearing Fish Xiphophorus Birchmanni. *J Hered* **106**, 57–66 (2015).

1033 79. E. Zeiske, R. Melinkat, H. Breucker, J. Kux, Ultrastructural studies on the epithelia of the
1034 olfactory organ of cyprinodonts (teleostei, cyprinodontoidea). *Cell Tissue Res.* **172**, 245–
1035 267 (1976).

1036 80. P. A. Triana-Garcia, "Studies on The Olfactory Biology and Behavioral Responses to Copper
1037 Exposure of The Native Indicator Species Delta Smelt (Hypomesus transpacificus)," UC
1038 Davis. (2021).

1039 81. P. A. Triana-Garcia, G. A. Nevitt, J. B. Pesavento, S. J. Teh, Gross morphology, histology,
1040 and ultrastructure of the olfactory rosette of a critically endangered indicator species, the
1041 Delta Smelt, Hypomesus transpacificus. *J Comp Physiol A Neuroethol Sens Neural Behav*
1042 *Physiol* **207**, 597–616 (2021).

1043 82. T. Shimizu, "Mucus, Goblet Cell, Submucosal Gland" in *Nasal Physiology and*
1044 *Pathophysiology of Nasal Disorders*, T. M. Önerci, Ed. (Springer, 2013), pp. 1–14.

1045 83. M. Lazzari, S. Bettini, L. Milani, M. G. Maurizii, V. Franceschini, Differential response of
1046 olfactory sensory neuron populations to copper ion exposure in zebrafish. *Aquatic*
1047 *Toxicology* **183**, 54–62 (2017).

84. K. E. Klima, F. M. Applehans, Copper exposure and the degeneration of olfactory receptors in rainbow trout (Oncorhynchus mykiss). *Chemical Speciation & Bioavailability* **2**, 149–154 (1990).

85. D. Saucier, L. Astic, Morpho-functional alterations in the olfactory system of rainbow trout (*Oncorhynchus mykiss*) and possible acclimation in response to long-lasting exposure to low copper levels. *Comparative Biochemistry and Physiology Part A: Physiology* **112**, 273–284 (1995).

86. Fish and Wildlife Service, US Department of the Interior, Endangered and Threatened Wildlife and Plants; 90-Day Finding on a Petition To List the Colorado River Cutthroat Trout. *Federal Register* **69**, 21151–21158 (2004).

87. N. H. Barton, K. S. Gale, "Genetic Analysis of Hybrid Zones" in *Hybrid Zones and the Evolutionary Process*, p. 33.

88. B.-J. Velthuis, W. Yang, T. Van Opijnen, J. H. Werren, Genetics of female mate discrimination of heterospecific males in *Nasonia* (Hymenoptera, Pteromalidae). *Animal Behaviour* **69**, 1107–1120 (2005).

89. O. Svensson, *et al.*, The genetics of mate preferences in hybrids between two young and sympatric Lake Victoria cichlid species. *Proceedings of the Royal Society B: Biological Sciences* **284**, 20162332 (2017).

90. E. M. Schmidt, K. S. Pfennig, Hybrid female mate choice as a species isolating mechanism: environment matters. *Journal of Evolutionary Biology* **29**, 865–869 (2016).

91. R. M. Paulette, Uno de los rostros de la migración interna. Marginación y pobreza en la sierra hidalguense. *Sociológica México* 157–191 (2015).

92. S. Cruz Hernández, *et al.*, Saberes tradicionales locales y el cambio climático global. *Revista mexicana de ciencias agrícolas* **11**, 1917–1928 (2020).

93. Y. Xia, C. Ti, D. She, X. Yan, Linking river nutrient concentrations to land use and rainfall in a paddy agriculture–urban area gradient watershed in southeast China. *Science of The Total Environment* **566–567**, 1094–1105 (2016).

94. E. Apeagyei, M. S. Bank, J. D. Spengler, Distribution of heavy metals in road dust along an urban-rural gradient in Massachusetts. *Atmospheric Environment* **45**, 2310–2323 (2011).

95. J. J. Sansalone, J. P. Hird, F. K. Cartledge, M. E. Tittlebaum, Event-Based Stormwater Quality and Quantity Loadings from Elevated Urban Infrastructure Affected by Transportation. *Water Environment Research* **77**, 348–365 (2005).

96. S. Yu, *et al.*, Anthropogenic land uses elevate metal levels in stream water in an urbanizing watershed. *Science of The Total Environment* **488–489**, 61–69 (2014).

97. V. Paul, M. S. Sankar, S. Vattikuti, P. Dash, Z. Arslan, Pollution assessment and land use land cover influence on trace metal distribution in sediments from five aquatic systems in southern USA. *Chemosphere* **263**, 128243 (2021).

98. D. H. Baldwin, C. P. Tatara, N. L. Scholz, Copper-induced olfactory toxicity in salmon and steelhead: Extrapolation across species and rearing environments. *Aquatic Toxicology* **101**, 295–297 (2011).

99. A. E. Smith, "The influence of sub-lethal zinc exposure on olfaction of alarm cues and associated alarm behaviours in juvenile coho salmon," University of British Columbia. (2023).

100. L. Sonnack, *et al.*, Effects of metal exposure on motor neuron development, neuromasts and the escape response of zebrafish embryos. *Neurotoxicology and Teratology* **50**, 33–42 (2015).

101. H. Tjälve, C. Mejàre, K. Borg-Neczak, Uptake and Transport of Manganese in Primary and Secondary Olfactory Neurones in Pike. *Pharmacology & Toxicology* **77**, 23–31 (1995).

102. Y. Rodríguez-Agudelo, *et al.*, Motor alterations associated with exposure to manganese in the environment in Mexico. *Science of The Total Environment* **368**, 542–556 (2006).

103. D. B. Szymkowicz, *et al.*, Exposure to arsenic during embryogenesis impairs olfactory sensory neuron differentiation and function into adulthood. *Toxicology* **420**, 73–84 (2019).

104. J. Lunt, D. L. Smee, Turbidity interferes with foraging success of visual but not chemosensory predators. *PeerJ* **3**, e1212 (2015).

105. S. M. Leahy, M. I. McCormick, M. D. Mitchell, M. C. O. Ferrari, To fear or to feed: the effects of turbidity on perception of risk by a marine fish. *Biology Letters* **7**, 811–813 (2011).

106. S. J. Song, B. Park, K. Jo, C.-S. Kim, Damage to Olfactory Organs of Adult Zebrafish Induced by Diesel Particulate Matter. *International Journal of Molecular Sciences* **23**, 407 (2022).

107. I. Reiten, *et al.*, Motile-Cilia-Mediated Flow Improves Sensitivity and Temporal Resolution of Olfactory Computations. *Current Biology* **27**, 166–174 (2017).

108. J. P. L. Cox, Hydrodynamic aspects of fish olfaction. *Journal of The Royal Society Interface* **5**, 575–593 (2008).

109. D. P. McEwen, P. M. Jenkins, J. R. Martens, "Chapter 12 Olfactory Cilia: Our Direct Neuronal Connection to the External World" in *Current Topics in Developmental Biology*, Ciliary Function in Mammalian Development., (Academic Press, 2008), pp. 333–370.

110. F. W. Sunderman, Nasal Toxicity, Carcinogenicity, and Olfactory Uptake of Metals. *Ann Clin Lab Sci* **31**, 3–24 (2001).